NUMERICAL MODELING OF SPACE PLASMA FLOWS / ASTRONUM-2007
ASP Conference Series, Vol. 385, ©2008
Nikolai V. Pogorelov, Edouard Audit, and Gary P. Zank, eds.

Magnetic Flux Conservation in Constrained Transport Adaptive Mesh MHD Codes Without Refluxing

Burlen Loring[1] and Joachim Raeder[1,2]

Abstract. The key property of constrained transport (CT) methods on fixed grids is that by design the equation $\nabla \cdot \mathbf{B} = 0$ is satisfied to within machine precision. However, when adaptive grids are introduced a naive treatment of magnetic flux conservation across the coarse–fine grid interface will lead to $\nabla \cdot \mathbf{B} \neq 0$ in coarse cells adjacent to refined regions. In this report we review the CT method for solving Faraday's law and present a new method for conserving magnetic flux across the coarse–fine grid interface. We show how magnetic flux can be conserved across the grid interface without a refluxing step. We then show a validation of our method, obtained with a new Adaptive Mesh Refinement (AMR) magnetohydrodynamic (MHD) code implemented with the CHOMBO AMR C++ classes.

1. Introduction

We present a new CT method for solving the equations of ideal MHD on block–structured adaptive (AMR) grids while automatically conserving magnetic flux across coarse–fine grid interfaces. Our method extends the constrained transport (CT) method of Evans & Hawley (1988) to incorporate the use of AMR methods introduced by Berger & Collela (1989). Previous work on extending CT for use on AMR grids followed a development strictly analogous to the development of hydrodynamic AMR given by Berger & Collela (1989), resulting in the inclusion of a curl-refluxing step (Balsara 2001). Our method differs from other block–structured AMR methods which incorporate CT in that it does not require a curl-refluxing step.

The equations of ideal MHD can be written as

$$\frac{\partial \mathbf{u}}{\partial t} + \nabla \cdot \mathbf{f}(\mathbf{u}) + \mathbf{A} = 0 \tag{1}$$

$$\frac{\partial \mathbf{B}}{\partial t} + \nabla \times \mathbf{E} = 0 \tag{2}$$

$$\nabla \cdot \mathbf{B} = 0, \tag{3}$$

where

$$\mathbf{u} = \begin{bmatrix} \rho \\ \rho\mathbf{v} \\ e_{\mathrm{T}} \end{bmatrix} \qquad \mathbf{f}(\mathbf{u}) = \begin{bmatrix} \rho\mathbf{v} \\ \rho\mathbf{v}\mathbf{v} + \mathbf{I}p \\ (e_{\mathrm{T}} + p)\mathbf{v} \end{bmatrix} \qquad \mathbf{A} = \begin{bmatrix} 0 \\ -\mathbf{j} \times \mathbf{B} \\ -\mathbf{j} \cdot \mathbf{E} \end{bmatrix}$$

[1]Institute for the Study of Earth Oceans and Space, University of New Hampshire, Durham, NH 03824

[2]University of New Hampshire, Department of Physics, Durham, NH 03824

$$p = (\gamma - 1)\left[e_{\rm T} - \frac{1}{2}\rho\mathbf{v}\cdot\mathbf{v}\right], \quad e_{\rm T} = \frac{\rho v^2}{2} + \frac{p}{\gamma - 1}, \quad \mathbf{j} = \nabla \times \mathbf{B}$$

and ρ is the fluid density, $\rho\mathbf{v}$ the momentum per unit volume, and $\mathbf{B}$ the magnetic field strength. The remaining variables are the derived quantities, p the gas pressure, $e_{\rm T}$ the sum of gas internal and kinetic energy per unit volume, and $\mathbf{j}$ the current density. It is this form of the ideal MHD equations which we will implement to test our new AMR CT method. Written this way, mass and magnetic flux are conserved; however momentum and energy are only conserved in the hydrodynamic sense (Raeder 2003).

In this report we only discuss numerics for equations (2) and (3). Although we have implemented the code using the above semi-conservative formulation, the CT method we have developed to conserve magnetic flux across AMR grid hierarchies can also be implemented using a fully conservative formulation of the ideal MHD equations simply by using our approach on equations (2) and (3) and adapting the momentum and energy equation to handle $\mathbf{B}$ on the staggered grid. We will not elaborate further on the choice of the semi-conservative formulation except to point the interested reader to the following sources that discuss various aspects of the formulation, namely: Brackbill & Barnes (1989), Janhunen (2000), Gombosi (2001), and Raeder (2003).

2. Faraday's Law: The Constrained Transport Method

The magnetic flux through the surface of one computational cell is given by

$$\Phi \equiv \iint \mathbf{B}\cdot d\mathbf{S}. \tag{4}$$

By virtue of Stokes's Theorem we can write the time change of Φ for each cell face as:

$$\frac{\partial\Phi}{\partial t} = \iint \frac{\partial\mathbf{B}}{\partial t}\cdot d\mathbf{S} = \iint (-\nabla\times\mathbf{E})\cdot d\mathbf{S} = -\oint \mathbf{E}\cdot d\mathbf{l}. \tag{5}$$

We discretize these integrals by placing components of $\mathbf{B}$ on cell faces, and components of $\mathbf{E}$ on the face edges, as shown in Figure 1. Here, and in the figures to follow, we introduce a general Cartesian coordinate system in the orthogonal basis vectors $\hat{\Theta}$,$\hat{\Psi}$,$\hat{\Omega}$. Discretized quantities are identified by the subscripts ijk. These subscripts when used with $\mathbf{B}$ and $\mathbf{E}$, identify the base face or base edge location respectively. Integer subscripts give the relative location with respect to the base edge or face; for example, $010 \equiv i, j+1, k$. Cell edge lengths are given by $\Delta\Theta$, $\Delta\Psi$, $\Delta\Omega$. Discretizing (5), we have the following expression for a single face

$$\begin{aligned}\left(\frac{\partial}{\partial t}B_{\Theta,ijk}\right)\Delta\Psi\Delta\Omega \\ = \quad -\left((E_{\Psi,ijk})\Delta\Psi + (E_{\Omega,010})\Delta\Omega - (E_{\Psi,001})\Delta\Psi - (E_{\Omega,ijk})\Delta\Omega\right),\end{aligned} \tag{6}$$

from which we arrive at the CT method of Evans and Hawley:

$$\frac{\partial}{\partial t}B_{\Theta,ijk} = -\left(\frac{E_{\Omega,010} - E_{\Omega,ijk}}{\Delta\Psi} - \frac{E_{\Psi,001} - E_{\Psi,ijk}}{\Delta\Omega}\right). \tag{7}$$

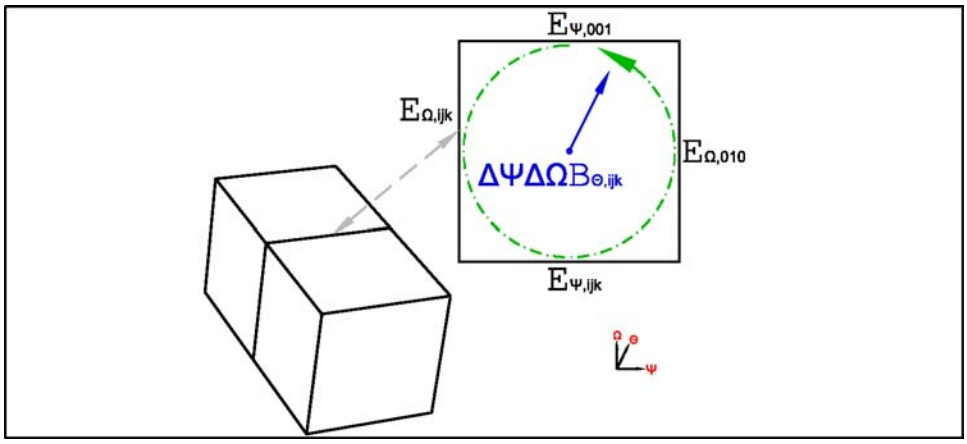

Figure 1. Adjacent computational cells with a shared face, shown in regular Cartesian coordinate system Θ, Ψ, Ω. Θ comes out of the page. Integer subscripts indicate addition to the base index ijk. $\mathbf{B}$ is located on the cell faces. $\mathbf{E}$ is located on the face edges.

Here any reasonable approach may be used to estimate $\mathbf{E}$ without affecting the divergence-free property of CT. We will compute $\mathbf{E}$ on face edges using the second–order monotonic upwind approach originally described in Evans & Hawley (1988) and compute the divergence of the magnetic field on a computational cell with

$$\nabla \cdot \mathbf{B} \approx \frac{B_{\Theta,100} - B_{\Theta,ijk}}{\Delta\Theta} + \frac{B_{\Psi,010} - B_{\Psi,ijk}}{\Delta\Psi} + \frac{B_{\Omega,001} - B_{\Omega,ijk}}{\Delta\Omega}. \tag{8}$$

A desirable feature of the CT method is that if $\nabla \cdot \mathbf{B} = 0$ initially it will grow, in the worst case, linearly at a rate given by the floating point round off error introduced per time step. Using rounding error estimation techniques of Goldberg (1991) we find that the order of rounding error per step, when using the second–order monotonic upwind approach, is on the order of 10ϵ, where $\epsilon = 2^{-52}$ for IEEE 754 double precision. Thus, given $\nabla \cdot \mathbf{B} = 0$ initially we can estimate the order of $\nabla \cdot \mathbf{B}$ at a later time by

$$O\left(\nabla \cdot \mathbf{B}|_{t=t_0+n\Delta t}\right) = 10n\epsilon O\left(max(|\mathbf{B}|)\right) \tag{9}$$

where n is the number of steps taken and the maximum should be taken over both space and time if $O(|\mathbf{B}|)$ changes over the time interval, and otherwise only spatially at $t = 0$.

3. Magnetic Flux Conservation at the Coarse-Fine Grid Interface

A crucial aspect of any divergence-free AMR implementation is that inter-level communications[3] must not introduce divergence. There are two possibilities.

[3]The interested reader may find an introduction to interlevel operations in (Berger & Collela 1989).

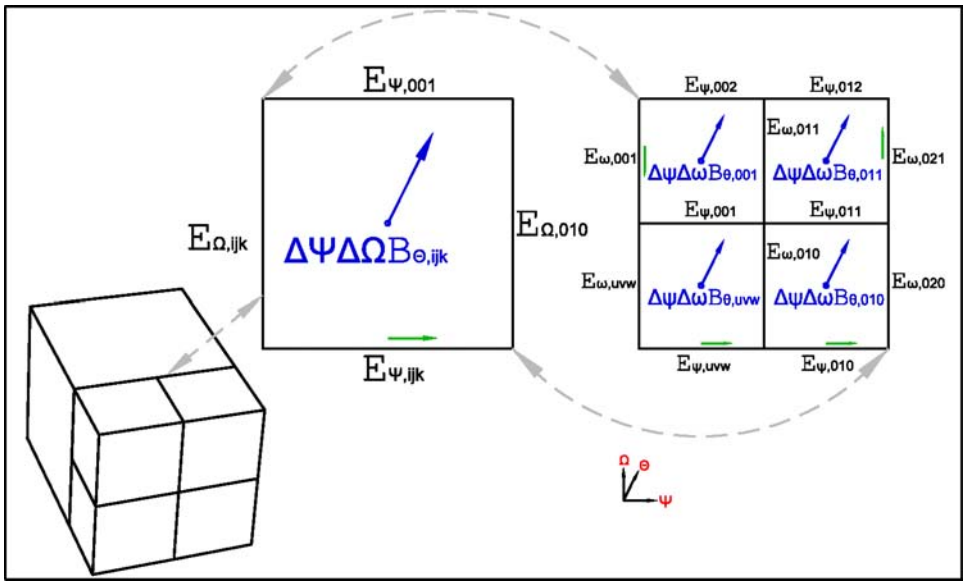

Figure 2. Coarse-fine grid interface. Four fine cells share a face with a coarse cell at the coarse fine grid interface, shown in regular Cartesian coordinate system Θ, Ψ, Ω where Θ comes out of the page. Integer subscripts indicate addition to the base index ijk (coarse grid) or uvw (fine grid). Components of $\mathbf{B}$ are located on the cell faces. Components of $\mathbf{E}$ are located on the face edges.

First, when coarse and fine grid solution become synchronous, where the coarse grid is covered by refined regions, the coarse grid is updated by a fine-to-coarse averaging procedure known as a restriction. Second, as the solution evolves and grids expand to cover previously unrefined areas, newly created refined grids are initialized via an interpolation from the coarse grid known as a prolongation. Both restriction and prolongation operations applied to $\mathbf{B}$ must be divergence-free if the solution is to have the divergence-free property. We have chosen to use the divergence-free restriction and prolongation formulas described in Toth & Roe (2002). The divergence-free prolongation is involved but straightforward, however the relatively simple restriction must be handled with care.

Applying the divergence theorem to (4) we see that

$$\Phi = \iint \mathbf{B} \cdot d\mathbf{S} = \iiint (\nabla \cdot \mathbf{B})\, dV = 0. \tag{10}$$

This equation explicitly illustrates the connection between magnetic flux conservation and the divergence-free condition on a computational cell. Note that after a restriction operation takes place, if flux has not been conserved across the coarse–fine grid interface, the divergence-free property of the coarse solution will be destroyed in cells that abut the refined region. This occurs in those cells due to the fact that the cell is divergence-free prior to the restriction, and that the restriction operation modifies the value of a single component of $\mathbf{B}$ on the face coincident with the coarse–fine grid interface, without changing the components of $\mathbf{B}$ on the other faces of that cell. In light of equation (10) the non-zero

divergence in these cells occurs due to a loss of magnetic flux conservation, in particular, at the coarse–fine grid interface. Thus, a non-zero divergence appearing in coarse cells which abut the coarse–fine grid interface indicates that magnetic flux has not been conserved across the coarse–fine grid interface.

In order to use the CT method with AMR grids, we must first address the issue of magnetic flux conservation across the coarse–fine grid interface. The situation is depicted in Figure 2. Θ, Ψ, Ω, ijk, and $\Delta\Theta$, $\Delta\Psi$, $\Delta\Omega$ are used to identify coordinate directions, base index, and computational cell edge lengths, respectively, on the coarse grid, while θ, ψ, ω, uvw, and $\Delta\theta$, $\Delta\psi$, $\Delta\omega$ are used for the same purpose on the fine grid. We introduce superscripts n and m to denote discrete temporal location on the coarse and fine grids respectively and we use a grid refinement ratio of 2. The conservation of magnetic flux across the coarse–fine grid interface implies that both

$$\Delta\Psi\Delta\Omega B^n_{\Theta,ijk} = \Delta\psi\Delta\omega\left(B^m_{\theta,uvw} + B^m_{\theta,010} + B^m_{\theta,001} + B^m_{\theta,011}\right) \tag{11}$$

and

$$\Delta\Psi\Delta\Omega B^{n+1}_{\Theta,ijk} = \Delta\psi\Delta\omega\left(B^{m+2}_{\theta,uvw} + B^{m+2}_{\theta,010} + B^{m+2}_{\theta,001} + B^{m+2}_{\theta,011}\right) \tag{12}$$

are satisfied. Given a grid refinement of 2, if the coarse and fine solutions are synchronous at a time specified by m and n, they will become synchronous again at the time specified by $n+1$ and $m+2$, due to the CFL restriction on the refined grid. We seek to construct a numerical scheme so that given (11), (12) is satisfied automatically. In other words we would like the time rate of change of the magnetic flux during the advance on the shared coarse–fine faces to be equivalent, specifically:

$$\begin{aligned}
&\Delta\Psi\Delta\Omega\frac{\partial}{\partial t}(B_{\Theta,ijk}) \\
&\quad = \quad \Delta\psi\Delta\omega\left(\frac{\partial}{\partial t}(B_{\theta,uvw}) + \frac{\partial}{\partial t}(B_{\theta,010}) + \frac{\partial}{\partial t}(B_{\theta,001}) + \frac{\partial}{\partial t}(B_{\theta,011})\right)
\end{aligned} \tag{13}$$

Here we must take into account that we evaluate the right side of (13) in 2 steps due to the CFL restriction, while the left side of (13) is obtained in a single step. Examining the lower-left face of the fine level we find that the magnetic field after two CT time steps is given by the expression:

$$\begin{aligned}
B^{m+2}_{\theta,uvw} &= B^m_{\theta,uvw} \\
&- \frac{\Delta t}{\Delta\psi\Delta\omega}\Big[(E^m_{\psi,uvw} + E^{m+1}_{\psi,uvw})\Delta\psi + (E^m_{\omega,010} + E^{m+1}_{\omega,010})\Delta\omega \\
&\qquad -(E^m_{\psi,001} + E^{m+1}_{\psi,001})\Delta\psi - (E^m_{\omega,uvw} + E^{m+1}_{\omega,uvw})\Delta\omega\Big].
\end{aligned} \tag{14}$$

Therefore by setting:

$$\left.\begin{array}{rcl} E^m_{\psi,uvw} & = & E^{m+1}_{\psi,uvw} \\ E^m_{\omega,010} & = & E^{m+1}_{\omega,010} \\ E^m_{\psi,001} & = & E^{m+1}_{\psi,001} \\ E^m_{\omega,uvw} & = & E^{m+1}_{\omega,uvw} \end{array}\right\}, \tag{15}$$

we obtain the desired result, a discretized expression for time change of magnetic flux on a particular fine level face over the time spanned by the coincident coarse face's time step, namely,

$$\Delta\psi\Delta\omega\left(\frac{B^{m+2}_{\theta,uvw}-B^{m}_{\theta,uvw}}{2\Delta t}\right) = -(E^{m}_{\psi,uvw}\Delta\psi + E^{m}_{\omega,010}\Delta\omega - E^{m}_{\psi,001}\Delta\psi - E^{m}_{\omega,uvw}\Delta\omega) \tag{16}$$

Substituting (6) for the left side of (13) and (16) and expressions like it for the other three fine faces into (13), we obtain

$$\begin{aligned} E^{n}_{\Psi,ijk}\Delta\Psi + E^{n}_{\Omega,010}\Delta\Omega - E^{n}_{\Psi,001}\Delta\Psi - E^{n}_{\Omega,ijk}\Delta\Omega \\ = (E^{m}_{\psi,uvw} + E^{m}_{\psi,010})\Delta\psi + (E^{m}_{\omega,020} + E^{m}_{\omega,021})\Delta\omega \\ -(E^{m}_{\psi,002} + E^{m}_{\psi,012})\Delta\psi - (E^{m}_{\omega,uvw} + E^{m}_{\omega,001})\Delta\omega. \end{aligned} \tag{17}$$

We can then equate coarse–fine terms which are coincident to arrive at the following set of conditions:

$$E^{n}_{\Psi,ijk}\Delta\Psi = (E^{m}_{\psi,uvw} + E^{m}_{\psi,010})\Delta\psi \tag{18}$$

$$E^{n}_{\Psi,001}\Delta\Psi = (E^{m}_{\psi,002} + E^{m}_{\psi,012})\Delta\psi \tag{19}$$

$$E^{n}_{\Omega,010}\Delta\Omega = (E^{m}_{\omega,020} + E^{m}_{\omega,021})\Delta\omega \tag{20}$$

$$E^{n}_{\Omega,ijk}\Delta\Omega = (E^{m}_{\omega,uvw} + E^{m}_{\omega,001})\Delta\omega \tag{21}$$

Equations (18)–(21) can be satisfied by setting:

$$\left.\begin{array}{lll} E^{m}_{\psi,uvw} & = & E^{m}_{\psi,010} = E^{n}_{\Psi,ijk} \\ E^{m}_{\psi,002} & = & E^{m}_{\psi,012} = E^{n}_{\Psi,001} \\ E^{m}_{\omega,020} & = & E^{m}_{\omega,021} = E^{n}_{\Omega,010} \\ E^{m}_{\omega,uvw} & = & E^{m}_{\omega,001} = E^{n}_{\Omega,ijk} \end{array}\right\}. \tag{22}$$

Thus we have the set of conditions, namely (15) and (22), which taken together guarantee that if we start with the flux conserved on cells which share faces across the coarse-fine grid interface, we will maintain flux conservation automatically during the time update. These are in essence a set of boundary conditions for the coarse–fine grid interface which we apply at each fine time step. In doing so we enforce the conservation of magnetic flux on the grid interface.

Before advancing the solution, we apply the conditions, (15) and (22), on the coarse-fine boundary insuring flux conservation during the advance. We treat the edges of the fine cell faces that are coincident with the coarse–fine grid interface as belonging to the ghost cells, interpolating from the coarse level there. This is reasonable because these edges are in fact part of the fine level ghost cells. A constant interpolation is reasonable for these edges because the edges of the fine cells on the coarse-fine interface are in fact spatially coincident with the coarse cell edges that are used as the source of the interpolation. The situation is depicted in Figure 3, where coarse–fine interface is shown on the left and the fine grid is shown on the right with its ghost cells. In contrast the traditional approach, proposed by Balsara (2001), is to advance the solution

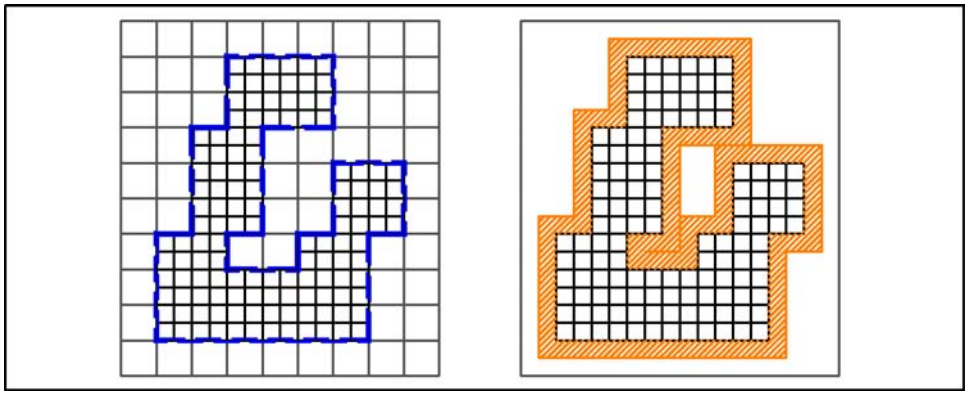

Figure 3. Hypothetical refined grid. On the left the coarse–fine interface is shown (thick broken line). On the right the fine grid is shown with its ghost cells. The ghost cells(hatched areas) are filled with information from the coarse grid.

first, then make a correction of the flux on the coarse cell faces using the flux calculated on the fine level. This process is known as curl-refluxing. We expect that our method produces similar results to the curl-refluxing approach. For both approaches flux across the coarse–fine interface, as calculated on the fine level, is calculated using information contained in the fine level ghost cells, which, except at the physical boundary of the problem space, contain at best coarse level accurate information. We posit that in most situations the affects on the solution due to using our approach are minimal compared to the traditional approach, however this remains to be shown. We emphasize that this paper represents a preliminary result. In future work we seek to quantify these results, examining a variety of situations that illustrate the strengths and weaknesses of our approach. For the present work we show that the method does what it says it will, conserve magnetic flux across the coarse–fine grid interface without a refluxing step.

4. Validation on an Adaptive Grid

We have implemented the algorithm using the CHOMBO AMR C++ classes (Colella 2007). The advantage of this choice is that CHOMBO handles the grid generation, interlevel operations for $\rho, \rho\mathbf{v}$, and e_{T} and provides aggregate data types for cell, face and edge located data. In addition to implementing the numerical algorithms we added divergence-free prolongation and restriction operators to CHOMBO. We present a cylindrical MHD blast problem as a preliminary validation of our approach. The MHD blast wave has been previously used as a validation on multidimensional MHD codes in Gardiner and Stone (2005). Additionally, if the strength of the initial disturbance is relatively small the exact position and shape of the resulting wavefronts can be determined analytically (Jeffrey 1966). In our solution the coarsest grid is composed of $100 \times 100 \times 3$

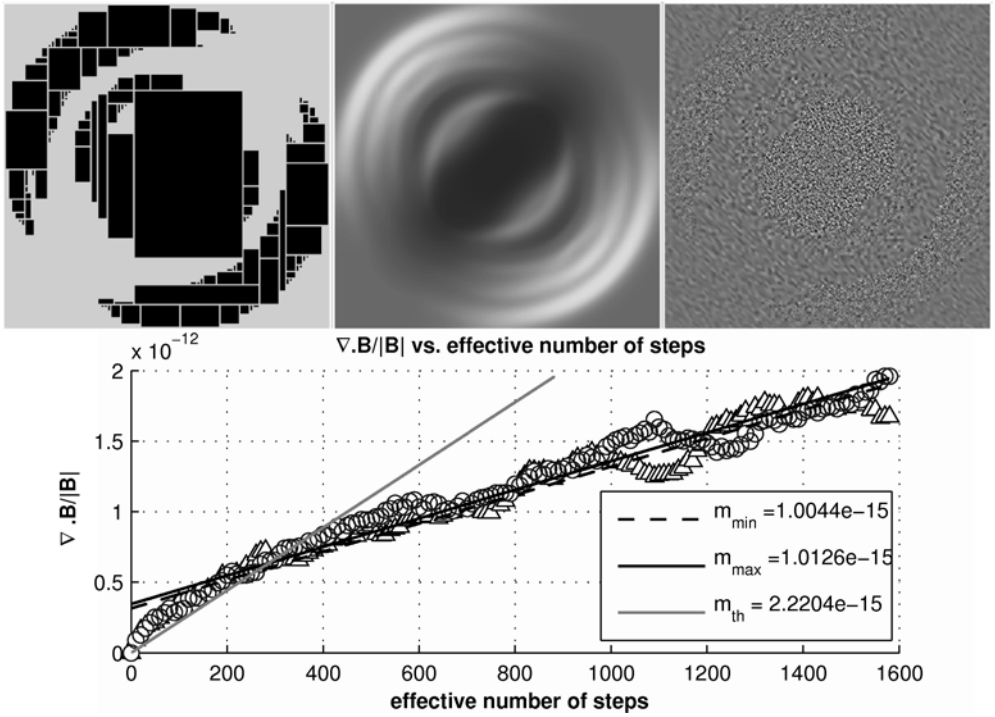

Figure 4. From left to right, on the top row: 1) Refined grid in black; 2) $|\mathbf{B}|$ varying from 9.64(dark) to 10.3 (light); and 3) $\nabla \cdot \mathbf{B}$ varying from -1.72E-11 (black) to 2.01E-11 (white). On the bottom row: 1) circles track $|\max \nabla \cdot \mathbf{B}|$ and triangles track $|\min \nabla \cdot \mathbf{B}|$, where both have been scaled by $|\mathbf{B}|$ and sampled at 10 step intervals; 2) Linear least squares fit(black lines) obtained using these data; and 3) light line shows the estimate given in equation(9).

cells, and spans -0.5 to 0.5 in the x-y plane. The initial conditions are given by:

$$(\rho, \mathbf{v}, \mathbf{B}, p) = \begin{cases} 1, 0, 0, 0, 10/\sqrt{2}, 10/\sqrt{2}, 0, 1 & \text{for } r \leq 0.1 \\ 1, 0, 0, 0, 10/\sqrt{2}, 10/\sqrt{2}, 0, 10 & \text{for } r > 0.1 \end{cases} \tag{23}$$

We run the code until the fast magnetosonic wave hits the boundary at $t = 0.038$. The results are shown in Figure 4. We show from left to right, top to bottom: 1) the refined grids, 2) $|\mathbf{B}|$, 3) $|\nabla \cdot \mathbf{B}|$, and 4) the growth of $\nabla \cdot \mathbf{B}$. We have tagged cells for refinement where, $0.09 \leq |\mathbf{v}| \leq 0.12$, and as a result the grids closely track the wavefronts propagating into the constant state. During this run we regrid at each step so that we are more likely to highlight any inconsistencies in our method. None were found. In the plot of $\nabla \cdot \mathbf{B}$ the refined region has a noticeably larger divergence than the unrefined region. This is expected as, compared to the unrefined region, twice the number of time steps have been taken on the refined region due to the tighter CFL restriction there. We note that $\nabla \cdot \mathbf{B} \approx 0$ including at the coarse–fine interface, which illustrates that we have indeed conserved magnetic flux across the interface. Also the slopes of the least squares lines show that growth of $\nabla \cdot \mathbf{B}$ is indeed of the order of magnitude predicted by (9).

5. Conclusion

In this report we introduced a method extending CT for use on AMR grids. We have shown that a refluxing step is not required to insure magnetic flux conservation across the coarse–fine grid interface if appropriate conditions are applied on the coarse–fine grid interface. We have also shown that our method works by applying it to a commonly found test problem, namely the MHD blast wave.

Acknowledgments. This work was supported by the National Aeronautics and Space Administration (NASA) Living With a Star (LWS) program under grant NNG04GP7 and by the National Science Foundation under grant ATM-0427754. Computations were performed at the San Diego Supercomputer Center (SDSC), the National Center for Supercomputer Applications (NCSA), and on the UNH Beowulf Cluster, which was in part funded by the Major Research Instrumentation (MRI) program of the National Science Foundation under grant ATM-0420905. We thank Dan Martin for advanced access to CHOMBO edge data C++ classes.

References

Balsara, D. 2001, J. Comput. Phys., 174, 614
Berger, M. J., & Collela, P. 1989, J. Comput. Phys., 82, 64
Brackbill, J. U., & Barnes, D. C. 1989, J. Comput. Phys., 1(35), 426
Colella, P., Graves, D. T., Keen,N. D., Ligocki, T. J., Martin, D. F., McCorquodale, P. W., Modiano, D., Schwartz, P. O., Sternberg, T. D., Van Straalen, B. 2007, Chombo Software Package for AMR Applications Design Document, Applied Numerical Algorithms Group, NERSC Division, Lawrence Berkeley National Laboratory Berkeley, CA
Evans, C., & Hawley, J. 1988, ApJ, 332, 659
Gardiner, T., & Stone, J. 2005, J. Comput. Phys., 205(2), 509
Goldberg, D. 1991, ACM Computing Surveys, 23(1), 5
DeZeeuw, D., Powell, K., Stout, Q., Gombosi, T., & Toth, G. 2001, in Proceedings of ISSS-6
Janhunen, P. 2000, J. Comput. Phys., 160, 649
Jeffrey, A. 1966, Magnetohydrodynamics (Edinbourg: Oliver & Boyd)
Raeder, J. 2003, in Space Plasma Simulation, ed. J. Büchner, C. T. Dum, & M. Scholer (Berlin: Springer)
Toth, G., & Roe, P. 2002, J. Comput. Phys., 180, 736